Criterion for the Electrical Resonance Stability of Offshore Wind Power Plants Connected through HVDC Links

Marc Cheah-Mane, *Student Member, IEEE*, Luis Sainz, Jun Liang, *Senior Member, IEEE*, Nick Jenkins, *Fellow, IEEE*, and Carlos E. Ugalde-Loo, *Member, IEEE*

***Abstract*—Electrical resonances may compromise the stability of HVDC-connected Offshore Wind Power Plants (OWPPs). In particular, an offshore HVDC converter can reduce the damping of an OWPP at low frequency series resonances, leading to system instability. The interaction between offshore HVDC converter control and electrical resonances of offshore grids is analyzed in this paper. An impedance-based representation of an OWPP is used to analyze the effect that offshore converters have on the resonant frequency of the offshore grid and on system stability. The positive-net-damping criterion, originally proposed for subsynchronous analysis, has been adapted to determine the stability of the HVDC-connected OWPP. The reformulated criterion enables the net-damping of the electrical series resonance to be evaluated and establishes a clear relationship between electrical resonances of the HVDC-connected OWPPs and stability. The criterion is theoretically justified, with analytical expressions for low frequency series resonances being obtained and stability conditions defined based on the total damping of the OWPP. Examples are used to show the influence that HVDC converter control parameters and the OWPP configuration have on stability. A root locus analysis and time-domain simulations in PSCAD/EMTDC are presented to verify the stability conditions.**

***Index Terms*—electrical resonance, offshore wind power plant, HVDC converter, positive-net-damping stability criterion.**

I. Introduction

HARMONIC instabilities have been reported in practical installations such as BorWin1, which was the first HVDC-connected Offshore Wind Power Plant (OWPP) [1], [2]. More recently, electrical interactions between offshore HVDC converters and series resonances have been identified in DolWin1 and highlighted by CIGRE Working Groups as potential causes of instability during the energization of the offshore ac grid [3], [4], [5]. Such interactions are known as electrical resonance instabilities [6]. In HVDC-connected OWPPs, the long export ac cables and the power transformers located on the offshore HVDC substation cause series resonances at low frequencies in the range of 100 $\sim$ 1000 Hz [3] - [5], [7]. Moreover, the offshore grid is a poorly damped system directly connected without a rotating mass or resistive loads [3], [2]. The control of the offshore HVDC converter can further reduce the total damping at the resonant frequencies until the system becomes unstable.

This work was supported in part by the People Programme (Marie Curie Actions) of the European Union's Seventh Framework Programme FP7/2007-2013/ (grant 317221 and project title MEDOW) and in part by the Ministerio de Economía y Competitividad (grant ENE2013-46205-C5-3-R).

M. Cheah-Mane, J. Liang, N. Jenkins and C.E. Ugalde-Loo are with the School of Engineering, Cardiff University, CF24 3AA Cardiff, UK. (e-mail: {CheahM, LiangJ1, JenkinsN6, Ugalde-LooC}@cardiff.ac.uk).

L. Sainz is with Electric Engineering Department, Universitat Politecnica de Catalunya (UPC), ETS d'Enginyeria Industrial de Barcelona, 08028 Barcelona, Spain (e-mail: sainz@ee.upc.edu).

Electrical resonance instability has been studied with an impedance-based representation by several authors. In [8], [9] Voltage Source Converters (VSCs) are modeled as Thévenin or Norton equivalents with a frequency-dependant characteristic. Nyquist and Bode criteria are used to analyze electrical resonance stability [2], [10]. In [9], a clear relationship between electrical resonances and the phase margin condition is established, but the complexity of the loop transfer function limits further analysis of the elements that cause instability. Alternative approaches, the passivity conditions of the system [11], [12] and the positive-net-damping criterion [13], [14], have been used to define stability conditions.

A number of studies on electrical resonance instability in OWPPs have been reported in the literature. In [15] and [16], the impact of electrical resonances on Wind Turbine (WT) converters is investigated. However, few studies are focused on the interactions between resonances and the offshore HVDC converter. In [17], a modal analysis in a HVDC-connected OWPP is used to characterize possible resonances and to assess the stability of the offshore converters. Also, in [9] and [18] the impact of resonances on offshore HVDC converters is analyzed using an impedance-based representation.

In this paper, the impact that low frequency series resonances have on the voltage stability of HVDC-connected OWPPs is analyzed and discussed. Preliminary work was reported in [19], where the stability criterion presented in this paper was assessed with examples. This paper furthers the initial contributions of [19] by providing a formal framework for the analysis of electrical resonance stability in HVDC-connected OWPPs. An impedance-based representation is used to identify resonances and to assess stability considering the effect of the offshore converters. The resonance stability of an OWPP is determined using an alternative approach to the positive-net-damping criterion [13]. This has been reformulated to evaluate the net-damping for electrical series resonances and to provide a clear relationship between electrical resonances of the OWPP and stability. The main contributions of this paper are summarized as follows:

- The alternative approach to the positive-net-damping criterion is demonstrated using the phase margin condition. This criterion defines the relation between the damping at electrical series resonances and system stability.
- The relationship between the total damping and resonant frequencies with the poles of the system is demonstrated. This relationship shows that the pole analysis and the positive-net-damping criterion provide the same information about resonance stability.

- Analytical expressions of the low frequency series resonances are proposed considering the effect of VSC controllers. These expressions are employed to calculate the resonant frequencies where the total damping is evaluated to determine system stability.
- A stable area of an OWPP is defined as a function of the HVDC converter control parameters and the OWPP configuration. Such an area is obtained from the damping of the OWPP and indicates conditions of stability.

The effect that the HVDC converter control parameters and the OWPP configuration have on stability is shown using examples. For completeness, root locus analysis and time-domain simulations in PSCAD/EMTDC are used to validate the stability conditions. The examples presented in this paper are complementary to those included in [19].

II. Impedance-based representation of an HVDC-connected OWPP

An impedance-based representation is suitable for the modeling of converters of an HVDC-connected OWPP whenever detailed design information is not available. Such a converter representation offers advantages as it can easily be combined with the equivalent impedance of the offshore ac grid to characterize resonant frequencies. It is also possible to consider the effect of the converter controllers. Moreover, the stability assessment methods for impedance-based representations are simple and less computational intensive compared to other traditional methods such as eigenvalue analysis [2], [10].

The configuration of an HVDC-connected OWPP is shown in Fig. 1. Type 4 WTs are connected to strings of the collector system through step-up transformers from low to medium voltage. Each WT grid side VSC has a coupling reactor and a high frequency filter represented as an equivalent capacitor. The strings are connected to a collector substation, where transformers step-up from medium to high voltage. The collector transformer in Fig. 1 is an equivalent representation of 4 transformers that are connected in parallel [3]. Export cables send the generated power to an offshore HVDC substation, where a VSC based Modular Multilevel Converter (MMC) operates as a rectifier and delivers the power to the dc transmission system. The dc transmission system and the onshore HVDC converters are not represented in this study.

Fig. 2 shows an impedance-based model of the HVDC-connected OWPP suitable for the analysis of electrical resonances and stability. The ac cables of the export and collector system are modeled as single π sections with lumped parameters and the transformers are modeled as RL equivalents. These models are accurate enough to characterize the low frequency resonances that are responsible for stability issues [3]. The VSCs are represented by equivalent circuits, which include the frequency response of the controller. The offshore VSC is represented by a Thévenin equivalent as it controls the ac voltage of the offshore grid [9], [20]; however, Norton equivalents are used to represent the WT VSCs since they control current [8], [20].

III. Impedance-based model of VSCs

The VSC models are represented in a synchronous dq frame and the Laplace s domain, where complex space vectors are

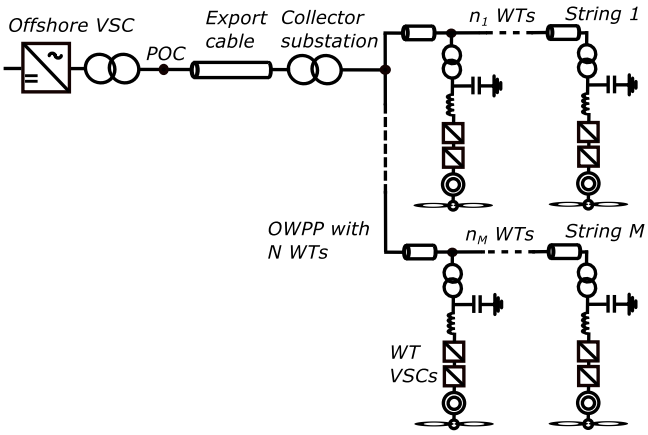

Fig. 1. General scheme of an HVDC-connected OWPP.

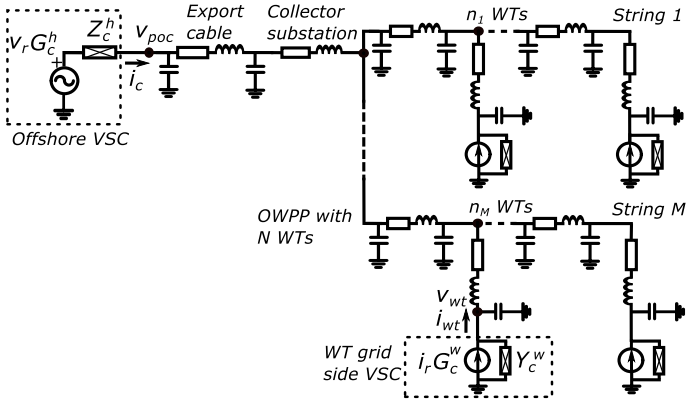

Fig. 2. Impedance-based model of an HVDC-connected OWPP for resonance and stability analysis.

denoted with boldface letters for voltages and currents as $\mathbf{v} = v_d + jv_q$ and $\mathbf{i} = i_d + ji_q$.

A. Offshore VSC model

The offshore VSC controls the ac voltage of the offshore grid. Fig. 3a describes the control structure of this converter. If the VSC uses a MMC topology, high frequency filters are not required and only a voltage control loop is considered [18], [21]. Additionally, the internal MMC dynamics can be neglected if a circulating current control is implemented [18]. A control action based on a PI controller is expressed as:

$$\mathbf{v_{vsc}^h} = F_{\mathrm{PI},v}(\mathbf{v_r} - \mathbf{v_{poc}}) \tag{1}$$

$$F_{\mathrm{PI},v} = k_{p,v} + \frac{k_{i,v}}{s} \tag{2}$$

where $\mathbf{v_{vsc}^h}$ is the reference voltage for the offshore converter, $\mathbf{v_r}$ is the control reference voltage at the Point of Connection (POC), $\mathbf{v_{poc}}$ is the voltage measured at the POC and $F_{\mathrm{PI},v}$ is the PI controller for the voltage control loop.

The dynamics across the equivalent coupling inductance of the offshore converter are expressed as:

$$\mathbf{v_{vsc}^h} = \mathbf{v_{poc}} + \mathbf{i_c}(R_f^h + sL_f^h + j\omega_1 L_f^h) \tag{3}$$

where $\mathbf{i_c}$ is the current from the HVDC converter, L_f^h is the coupling inductance, R_f^h is the equivalent resistance of L_f^h and $\omega_1 = 2\pi f_1$ rad/s (f_1 = 50 Hz). The coupling inductance is equal to $L_f^h = L_{arm}/2 + L_{tr}^h$, where L_{arm} is the arm

inductance of the MMC and L_{tr}^h is the equivalent inductance of the offshore HVDC transformers.

A Thévenin equivalent of the offshore VSC (see Fig. 2) is obtained by combining (1) and (3):

$$\mathbf{v_{poc}} = \mathbf{v_r} \cdot G_c^h - \mathbf{i_c} \cdot Z_c^h \tag{4}$$

$$G_c^h = \frac{F_{\mathrm{PI},v}}{1 + F_{\mathrm{PI},v}};\ Z_c^h = \frac{R_f^h + sL_f^h + j\omega_1 L_f^h}{1 + F_{PI,v}} \tag{5}$$

where G_c^h is the voltage source transfer function and Z_c^h is the input-impedance of the converter.

B. Wind Turbine VSC model

Each WT is equipped with a back-to-back converter, but only the grid side VSC is represented in this study. Its control is based on an ac current loop employing a PI controller as shown in Fig. 3b. The dc voltage outer loop is not represented in the WT VSC model since its dynamic response is slow; *i.e.* there is sufficient bandwidth separation with the inner current loop [2], [22]. This ensures that there are no interactions between harmonic resonances and the outer loops, which are not of interest in this paper. A Norton equivalent of the WT converter (see Fig. 2) is obtained as:

$$\mathbf{i_{wt}} = \mathbf{i_r} \cdot G_c^w - \mathbf{v_{wt}} \cdot Y_c^w \tag{6}$$

where $\mathbf{i_{wt}}$ is the current from the WT VSC, $\mathbf{i_r}$ is the control reference current, G_c^w is the current source transfer function, $\mathbf{v_{wt}}$ is the voltage after the coupling filter and Y_c^w is the input-admittance of the VSC. G_c^w and Y_c^w are expressed as [8]:

$$G_c^w = \frac{F_{\mathrm{PI},c}}{R_f^w + sL_f^w + F_{\mathrm{PI},c}};\ Y_c^w = \frac{1 - H_v}{R_f^w + sL_f^w + F_{\mathrm{PI},c}} \tag{7}$$

$$F_{\mathrm{PI},c} = k_{p,c} + \frac{k_{i,c}}{s};\ H_v = \frac{\alpha_f}{s + \alpha_f} \tag{8}$$

where $F_{\mathrm{PI},c}$ is the PI controller of the current loop, L_f^w the coupling inductance, R_f^w the equivalent resistance of L_f^w, H_v the low pass filter of the voltage feed-forward term [8] and α_f the bandwidth of H_v. The PI design is based on [8], [23], with proportional and integral gains given as $k_{p,c} = \alpha_c L_f^w$ and $k_{i,c} = \alpha_c R_f^w$, and the bandwidth of the current control by α_c.

IV. Stability analysis of HVDC-connected OWPPs

The stability analysis considers the impedance-based circuit presented in Fig. 4, where the offshore grid is modeled with an equivalent circuit (further explained in Section V). A similar representation can be found in [9].

The impedances were expressed in the stationary $\alpha\beta$ frame [6], [11], which is denoted in boldface letters for voltages and currents as $\mathbf{v^s} = v_\alpha + jv_\beta$ and $\mathbf{i^s} = i_\alpha + ji_\beta$. The current in the stationary $\alpha\beta$ frame and the Laplace *s*-domain is given as:

$$\mathbf{i_c^s} = (\mathbf{v_r^s} G_c^h - \mathbf{i_r^s} G_c^w Z_c^w) \overbrace{\frac{1/Z_g}{1 + Z_c^h/Z_g}}^{T^h} \tag{9}$$

where $Z_g = Z_{eq}^{grid} + 1/Y_c^w$ is the equivalent impedance of the OWPP from the offshore VSC and T^h is the OWPP closed loop transfer function, which can be also expressed as:

$$T^h(s) = \frac{M(s)}{1 + M(s)N(s)} = \frac{M(s)}{1 + L(s)} \tag{10}$$

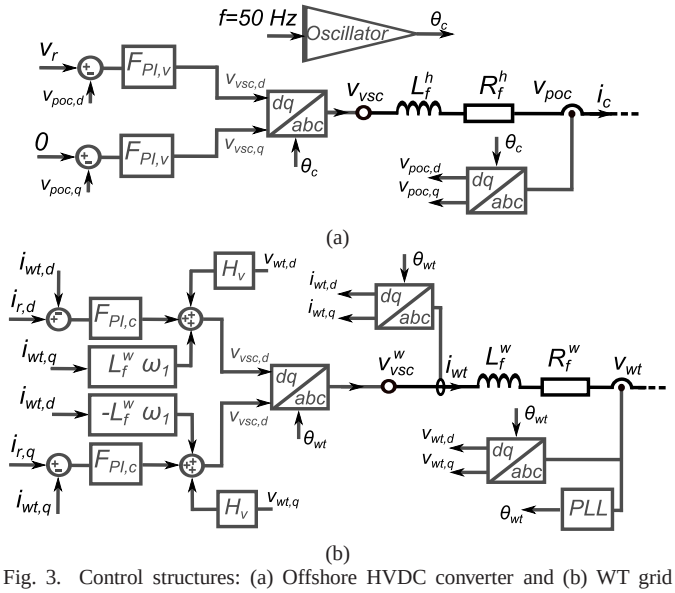

Fig. 3. Control structures: (a) Offshore HVDC converter and (b) WT grid side converter.

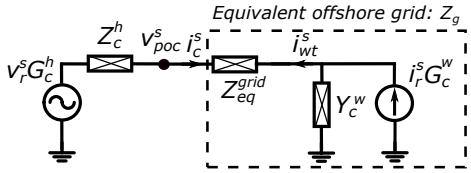

Fig. 4. Equivalent impedance-based circuit of an HVDC-connected OWPP with representation of offshore grid circuit.

where $M(s) = 1/Z_g$ is the open loop transfer function, $N(s) = Z_c^h$ is the feedback transfer function and $L(s)$ is the loop transfer function.

Assuming that the voltage and current sources in Fig. 4 are stable when they are not connected to any load [10], the stability of the OWPP can be studied in the following ways:

- By analyzing the poles of T^h or the roots of $Z_g + Z_c^h = 0$.
- By applying the Nyquist stability criterion of Z_c^h/Z_g [10].
- By considering the passivity of T^h [6], [11].

In addition to the previous alternatives, a variation to the positive-net-damping criterion given in [13], [14] is here employed instead to analyze system stability. The criterion has been reformulated to evaluate electrical resonance stability as explained in section IV-B.

A. Passivity

A linear and continuous-time system $F(s)$ is passive if [11]:

- $F(s)$ is stable and,
- $\mathrm{Re}\{F(j\omega)\} > 0\ \forall\ \omega$, which is expressed in terms of the phase as $-\frac{\pi}{2} < \arg\{F(j\omega)\} < \frac{\pi}{2}$. This condition corresponds to a non-negative equivalent resistance in electrical circuits.

Passivity can be applied to determine the stability of closed loop systems [6], [11]. A system represented by the closed loop transfer function in (10) is stable if $M(s)$ and $N(s)$ are passive since $-\pi < \arg\{L(j\omega)\} < \pi\ \forall\ \omega$. This implies that the Nyquist stability criterion for $L(s)$ is satisfied. Therefore, the OWPP is stable if Z_g and Z_c^h are passive. When the HVDC converter is connected to a passive offshore grid, Z_g is passive

and the stability only depends on the passivity conditions of the converter input-impedance, Z_c^h.

In no-load operation (*i.e.* when only the passive elements of the OWPP are energized), the passivity of Z_g is ensured as the WTs are assumed to be disconnected from the offshore grid. However, the WTs represent active elements when they are connected to the offshore grid (*i.e.* Z_g can have a negative resistance), which may compromise the OWPP stability.

B. Positive-net-damping stability criterion

The criterion states that a closed loop system is stable if the total damping of the OWPP is positive at the following frequencies: (i) open loop resonant frequencies and (ii) low frequencies where the loop gain is greater than 1 [13]. However, it does not provide a clear relation between electrical resonances of the OWPP and system stability. This increases the complexity of analyzing the impact that system parameters have on resonance stability.

The criterion presented in [13] has been reformulated to evaluate the net-damping for electrical series resonances. The approach proposed in this paper is developed from the phase margin condition [9]. If stability is evaluated in terms of the phase margin, $L(j\omega) = M(j\omega)N(j\omega)$ must satisfy the following conditions at angular frequency ω:

$$|M(j\omega)N(j\omega)| = 1, \tag{11}$$

$$-\pi < \arg\{M(j\omega)N(j\omega)\} < \pi \ \forall\ \omega. \tag{12}$$

$M(j\omega)$ and $N(j\omega)$ in (11) and (12) can be expressed in terms of equivalent impedances as:

$$\frac{1}{M(j\omega)} = Z_g(j\omega) = R_g(\omega) + jX_g(\omega) \tag{13}$$

$$N(j\omega) = Z_c^h(j\omega) = R_c^h(\omega) + jX_c^h(\omega) \tag{14}$$

Also, the equivalent impedance from the voltage source $\mathbf{v_r^s}G_c^h$ in Fig. 4 is expressed as:

$$Z_{eq}^h(j\omega) = Z_c^h(j\omega) + Z_g(j\omega) \tag{15}$$

Phase margin condition (11) is equivalent to:

$$R_c^h(\omega)^2 + X_c^h(\omega)^2 = R_g(\omega)^2 + X_g(\omega)^2 \tag{16}$$

The resistive components in ac grids and VSCs may be usually neglected compared to the reactive components. Therefore, $R_g \ll X_g$, $R_c^h \ll X_c^h$ and (16) is simplified to:

$$X_c^h(\omega) = \pm X_g(\omega) \tag{17}$$

The electrical series resonances observed from the voltage source $\mathbf{v_r^s}G_c^h$ in Fig. 4 correspond to frequencies where Z_{eq}^h in (15) has a dip or a local minimum. If the resistive components are neglected, the series resonance condition is reduced to:

$$\mathrm{Im}\{Z_{eq}^h(j\omega_{res})\} \approx 0 \Rightarrow X_c^h(\omega_{res}) \approx -X_g(\omega_{res}) \tag{18}$$

It can be observed that (18) is a particular case of (17); *i.e.* the series resonance condition of Z_{eq}^h coincides with the stability condition $|M(j\omega)N(j\omega)| = 1$ given by (11).

Phase margin condition (12) can be expressed in terms of the imaginary part of $L(j\omega)$ as follows:

$$\begin{cases} \text{If } \frac{d|L(j\omega)|}{d\omega} > 0: \ 0 < \arg\{L(j\omega)\} < \pi \Rightarrow \\ \qquad \Rightarrow R_g(\omega)X_c^h(\omega) - R_c^h(\omega)X_g(\omega) > 0 \\ \text{If } \frac{d|L(j\omega)|}{d\omega} < 0: \ -\pi < \arg\{L(j\omega)\} < 0 \Rightarrow \\ \qquad \Rightarrow R_g(\omega)X_c^h(\omega) - R_c^h(\omega)X_g(\omega) < 0 \end{cases} \tag{19}$$

If the resonance condition in (18) is combined with (19):

$$\begin{cases} \text{If } \frac{d|L(j\omega)|}{d\omega} > 0 : X_c^h(\omega_{res})[R_g(\omega_{res}) + R_c^h(\omega_{res})] > 0 \\ \text{If } \frac{d|L(j\omega)|}{d\omega} < 0 : X_c^h(\omega_{res})[R_g(\omega_{res}) + R_c^h(\omega_{res})] < 0 \end{cases} \tag{20}$$

It can be shown (see Appendix A) that if the offshore grid is capacitive (*i.e.* $X_g < 0$) and the HVDC converter is inductive (*i.e.* $X_c^h > 0$), then $\frac{d|L(j\omega)|}{d\omega} > 0$. On the other hand, if the offshore grid is inductive (*i.e.* $X_g > 0$) and the HVDC converter is capacitive (*i.e.* $X_c^h < 0$), then $\frac{d|L(j\omega)|}{d\omega} < 0$. By considering the previous conditions, (20) is simplified to:

$$R_T(\omega_{res}) = R_g(\omega_{res}) + R_c^h(\omega_{res}) > 0 \tag{21}$$

where resistance R_T represents the total damping of the system, resistance R_c^h the HVDC converter damping and resistance R_g the offshore grid damping.

It can be observed that (21) is equivalent to the positive-net-damping criterion in [13], but evaluated for the series resonances of Z_{eq}^h. Therefore, the offshore HVDC VSC is asymptotically stable if the total damping of the system, R_T, is positive in the neighborhood of an electrical series resonance. The advantage of this criterion with respect to the passivity approach is that the stability can be ensured even if Z_g and Z_c^h are not passive because it considers the contribution of both terms in the closed loop system.

It should be noted that if the resistive components of the offshore grid and HVDC VSC are large compared to the reactive elements (*e.g.* $X_g/R_g < 10$ and $X_c^h/R_c^h < 10$), the approximations in (17) and (18) are not valid and this criterion cannot be used.

C. Relation between total damping and poles of the system

The HVDC-connected OWPP is a high order system with several poles. However, the system response is governed by a dominant poorly-damped pole pair. If this pole pair is related to the electrical series resonance, impedances Z_c^h and Z_g around this resonance can be approximated as:

$$Z_{c,res}^h(s) \approx R_c^h + sL_c^h;\ Z_{g,res}(s) \approx R_g + \frac{1}{sC_g} \tag{22}$$

where C_g is the equivalent capacitor of the offshore grid impedance when the frequency is close the resonance. Using (18), the series resonance reduces to $\omega_{res} = 1/\sqrt{L_c^h C_g}$.

The poles related to the series resonance are obtained from $1 + Z_{c,res}^h(s)/Z_{g,res}(s) = 0$, yielding:

$$s = \frac{-(R_c^h + R_g)C_g \pm \sqrt{(R_c^h + R_g)^2 C_g^2 - 4L_c^h C_g}}{2L_c^h C_g} \tag{23}$$

Considering that $(R_c^h + R_g)^2 C_g^2 \ll 4L_c^h C_g$, equation (23) is approximated to:

$$s \approx -\frac{R_c^h + R_g}{2L_c^h} \pm j\frac{1}{\sqrt{L_c^h C_g}} \tag{24}$$

The imaginary part of the closed loop system poles corresponds to the resonant frequency. Also, the real part of the poles is correlated to the total damping, $R_c^h + R_g$, as mentioned in [14]. Therefore, there is a pair of poles that represent the series resonance and can be used to identify instabilities.

V. Resonance characterization

In this section, the low frequency series resonances of an OWPP are characterized. It is useful to identify resonant frequencies in an OWPP since they can destabilize an offshore HVDC converter. To this end, the frequency response of $Z^h_{eq}(j\omega)$ is here used to identify electrical resonances. Due to the complexity of the VSC and offshore grid equations, simplifications are used to obtain analytical expressions of the resonant frequencies.

A. Simplifications of the OWPP impedance model

Fig. 5 shows that the frequency response of a VSC impedance can be simplified to RL equivalents above 100 Hz. The input-impedance of the VSCs was represented in an $\alpha\beta$ frame (see Fig. 4). To achieve this, a reference frame transformation from dq to $\alpha\beta$ was performed using the rotation $s \rightarrow s - j\omega_1$ [6], [15]. For frequencies higher than ω_1, the offshore VSC impedance, $Z^h_c(s - j\omega_1)$, is approximated to:

$$R^h_c = \frac{R^h_f}{1 + k_{p,v}}; \quad L^h_c = \frac{L^h_f}{1 + k_{p,v}} \tag{25}$$

Similarly, the WT VSC impedance, $Z^w_c(s-j\omega_1) = 1/Y^w_c(s-j\omega_1)$, is approximated to:

$$R^w_c = R^w_f + (\alpha_f + \alpha_c)L^w_f; \quad L^w_c = L^w_f \tag{26}$$

The previous simplifications do not consider the VSCs as active elements since R^h_c and R^w_c are positive for all frequencies.

Fig. 6 shows the equivalent model of the HVDC-connected OWPP with the simplified VSC and cable models. The capacitor C_{ec} represents the export cable capacitance. The inductive and resistive components of the export cable are small enough to be combined with the RL equivalent of the transformers and the HVDC converter. Also, the collector cables are removed because their equivalent inductance and capacitance are small and only affect the response at high frequencies, which are not considered in this study.

When the collector cables are removed, the aggregation of WTs is reduced to a combination of parallel circuits independent to the collector system topology. Fig. 7 shows the OWPP model under this scenario, which is equivalent to the model in Fig. 4. The parameters of the aggregated model are defined as follows:

- R^{cs}_{tr} and L^{cs}_{tr} are the RL values of the collector transformers.
- $R^w_{tr,a}$ and $L^w_{tr,a}$ are the RL values of the aggregated WT transformers:

$$R^w_{tr,a} = R^w_{tr}/N \; ; L^w_{tr,a} = L^w_{tr}/N \tag{27}$$

  where N is the number of WTs and R^w_{tr} and L^w_{tr} are the RL values of one WT transformer.
- $R^w_{c,a}$ and $L^w_{c,a}$ are the RL values of the aggregated WT converters:

$$R^w_{c,a} = R^w_c/N \; ; L^w_{c,a} = L^w_c/N \tag{28}$$

- $C^w_{f,a}$ is the equivalent capacitance of the aggregated WT low pass filters:

$$C^w_{f,a} = C^w_f \cdot N \tag{29}$$

where C^w_f is the capacitance of one WT low pass filter.

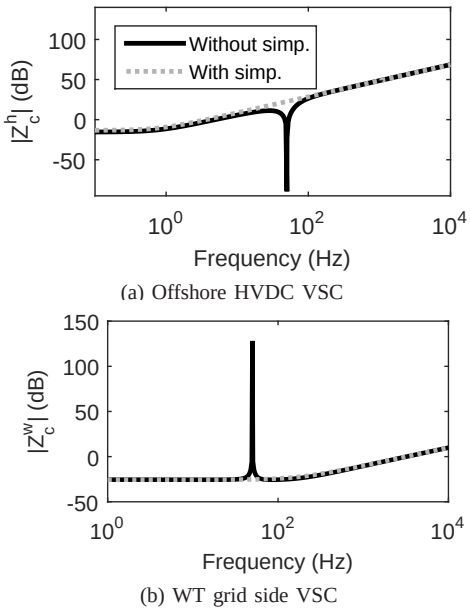

Fig. 5. Frequency response with and without simplifications (parameters in Appendix B with $k_{p,v}$= 1, $k_{i,v}$= 500).

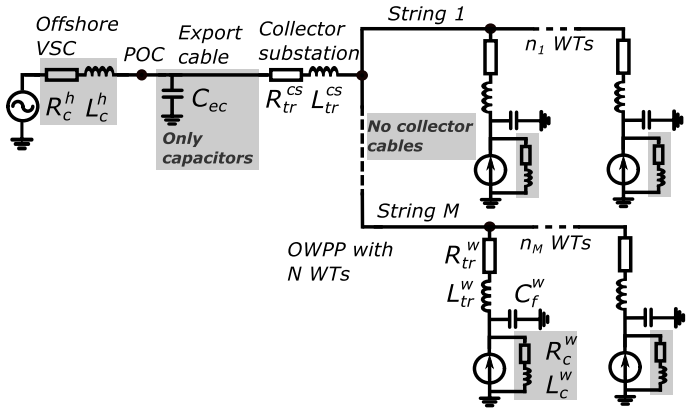

Fig. 6. Impedance-based model of an HVDC-connected OWPP with simplified VSC and cable models (indicated in grey rectangles).

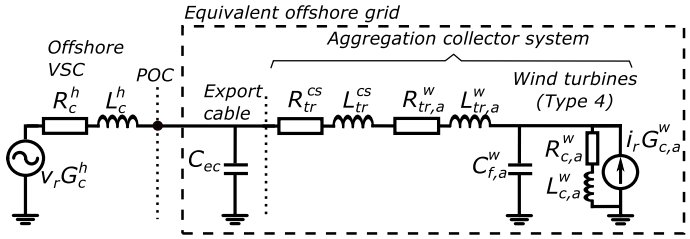

Fig. 7. Impedance-based model of an HVDC-connected OWPP with aggregation of collector system.

Fig. 8 shows the frequency response of the equivalent offshore grid impedance, Z^h_{eq}, with and without simplifications to VSC and cable models. It can be observed that if simplifications are made the 50 Hz resonance of the VSC control is not exhibited; however, the frequency response agrees well with that of the un-simplified Z^h_{eq} over 200 Hz and up to 1 kHz.

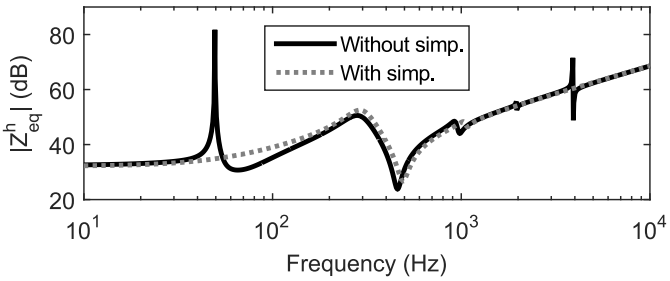

Fig. 8. Frequency response of OWPP impedance without and with VSC and cable simplifications (parameters in Appendix B and $k_{p,v}$= 1, $k_{i,v}$= 500).

Additionally, the simplification of the collector cables slightly shifts the series resonance from 459 Hz to 497 Hz. In light of these results, it can be concluded that the simplified frequency response represents a good approximation for low frequency resonances in the range of 200 $\sim$ 1000 Hz.

B. Analytical expression for the series resonant frequency

The expression of the lowest series resonant frequency of Z^h_{eq} is obtained for no-load operation and when WTs are connected. The resistances are neglected as they only have a damping effect on resonance (*i.e.* they barely modify the resonant frequency).

In no-load operation, the WTs are not connected and the contribution of the collector system at low frequencies is negligible. Therefore, the OWPP impedance Z^h_{eq} in (15) is equivalent to an LC circuit with a resonant frequency:

$$f_{res}^{nload} = \frac{1}{2\pi\sqrt{L^h_c C_{ec}}} \tag{30}$$

The lowest series resonant frequency when WTs are connected has been obtained following an algebraic calculation using Fig. 7:

$$\begin{cases} f_{res}^{load} = \dfrac{1}{2\pi}\sqrt{\dfrac{b-\sqrt{b^2-4ad}}{2a}} \\ a = C_{ec}L^w_{c,a}(L^{cs}_{tr}+L^w_{tr,a})L^h_c C^w_{f,a} \\ b = C_{ec}L^h_c(L^w_{c,a}+L^{cs}_{tr}+L^w_{tr,a})+ \\ \quad +C^w_{f,a}L^w_{c,a}(L^h_c+L^{cs}_{tr}+L^w_{tr,a}) \\ d = L^h_c+L^w_{c,a}+L^{cs}_{tr}+L^w_{tr,a} \end{cases} \tag{31}$$

Expressions (30) and (31) are employed to calculate the frequencies where the total system damping is evaluated to determine stability.

VI. Voltage Stability Analysis

The modified positive-net-damping criterion was applied to analyze the impact of electrical series resonances in the voltage stability of an HVDC-connected OWPP. The effects of the offshore HVDC converter control and the OWPP configuration are considered in the study. For completeness, the root locus of the system and time-domain simulations in PSCAD/EMTDC are used to confirm the results.

The cable model simplifications considered in the resonance characterization are used in the stability analysis given that the low frequency response is well-represented and the damping contribution from the cable resistances can be neglected. However, the VSC simplifications in (25) and (26) are not considered, because the converters are not represented as active elements. The system is analyzed in no-load operation and when WTs are connected based on the OWPP described in Appendix B.

A. No-load operation

In no-load operation, the positive-net-damping stability criterion only includes the damping contribution of the offshore converter, R^h_c, because the export and collector cables are passive elements with a small resistance and thus can be neglected (*i.e.* $R_g \approx 0$). Therefore, condition (21) is reduced to $R^h_c(\omega_{res}) > 0$, which is equivalent to analyzing the passivity of the HVDC converter control at a resonant frequency.

Stability is ensured if the electrical series resonance is located in a frequency region with positive resistance. This region is determined using the zero-crossing frequencies of R^h_c (*i.e.* $R^h_c(\omega) = \mathrm{Re}\{Z^h_c(\omega)\} = 0$) in (5). The two following solutions are obtained:

$$\begin{cases} \omega_{cut1} = \omega_1 = 2\pi(50) \\ \omega_{cut2} = \dfrac{\omega_1}{1-\dfrac{k_{i,v}L^h_f}{R^h_f(1+k_{p,v})}} \end{cases} \tag{32}$$

When $\omega_{cut2} < 0$, the only zero-crossing frequency considered is 50 Hz and R^h_c is negative for $\omega > 2\pi(50)$. Therefore, the converter is always unstable for resonant frequencies above 50 Hz. If $\omega_{cut2} > 0$, then R^h_c is negative for $2\pi(50) < \omega < \omega_{cut2}$ and positive for $\omega > \omega_{cut2}$. In this case, the converter is stable for frequencies higher than ω_{cut2} since the resonance is located in a positive-resistance region. Thus, the offshore HVDC converter is stable when R^h_c has two zero-crossing frequencies ($\omega_{cut2} > 0$ and $\omega_{res} > \omega_{cut2}$). The following inequalities are obtained by combining (30) and (32):

$$\begin{cases} \omega_{cut2} > 0 \Rightarrow \;\; R^h_f(1+k_{p,v}) - k_{i,v}L^h_f > 0 \\ \omega_{res} > \omega_{cut2} \Rightarrow \;\; R^{h2}_f(1+k_{p,v})^2 - 2R^h_f L^h_f(1+k_{p,v})k_{i,v} - \\ \qquad\qquad -\omega_1^2 R^{h2}_f L^h_f C_{ec}(1+k_{p,v}) + k^2_{i,v}L^{h2}_f > 0 \end{cases} \tag{33}$$

Fig. 9 shows the stability area ($R^h_c(\omega_{res}) > 0$) defined by (33) as a function of the control parameters of the offshore HVDC converter, $k_{p,v}$ and $k_{i,v}$, and the export cable length, l_{cb}. It is observed that when the cable length increases the stable area is reduced.

Fig. 10 shows the root locus of the low frequency resonant poles for parametric variations of $k_{p,v}$, $k_{i,v}$ and l_{cb}. It should be emphasized that these poles are not complex conjugate due to the transformation of the VSC input impedance from a synchronous dq to a stationary $\alpha\beta$ reference frame, which introduces complex components. The increase of cable length moves the resonance to lower frequencies since C_{ec} increases. As $k_{p,v}$ increases, the resonance shifts to higher frequencies given that L^h_c in (25) decreases. Changes in $k_{i,v}$ do not affect the resonant frequency. The system becomes unstable when one of the resonant poles moves to the positive side of the real axis; this is equivalent to have a negative damping. It can be observed that the stability conditions of the resonant poles agree with the stable areas shown in Fig. 9.

Figs. 11 and 12 show examples of stable and unstable cases when $k_{i,v}$ is modified. The intersection between Z^h_c

This article has been accepted for publication in a future issue of this journal, but has not been fully edited. Content may change prior to final publication. Citation information: DOI 10.1109/TPWRS.2017.2663111, IEEE Transactions on Power Systems

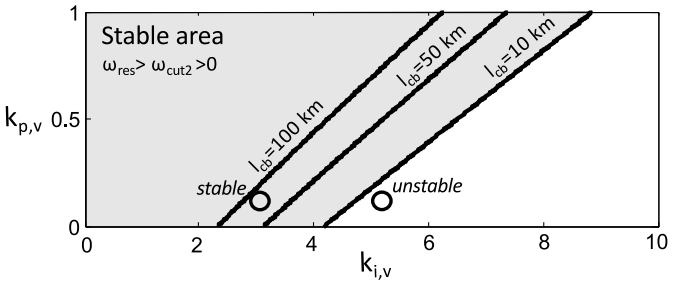

Fig. 9. Stable area of offshore HVDC converter in no-load operation as function of $k_{p,v}$, $k_{i,v}$ and l_{cb} (the stable and unstable examples of Fig. 11 and 12 are marked with circles).

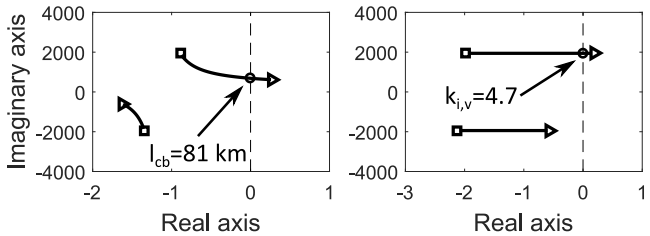

(a) Cable length variation from 1 to 100 km ($k_{p,v} = 0.1$, $k_{i,v} = 3$).

(b) Variation of $k_{i,v}$ from 1 to 5 ($k_{p,v} = 0.1$, $l_{cb} = 10$ km).

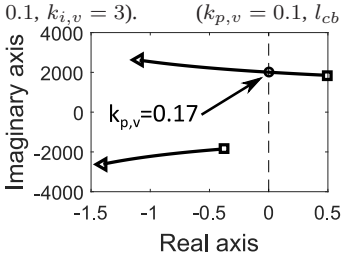

(c) Variation of $k_{p,v}$ from 0 to 1 ($k_{i,v} = 5$, $l_{cb} = 10$ km)

Fig. 10. Root locus of OWPP in no-load operation for variations of export cable length and ac voltage control parameters.

and Z_g (*i.e.* $1/|M(j\omega)| = |N(j\omega)|$) approximately determines the series resonant frequency, as defined in (18). When the system is stable the resonant frequency is located in a positive-resistance region of Z_c^h, as shown in Fig. 11a. Also, following the Nyquist criterion, the Nyquist curve encircles $(-1, 0)$ in anti-clockwise direction and the open loop system does not have unstable poles. Therefore, the system is stable as it does not have zeros with positive real part. Although the ac voltage control can be designed to ensure stability, all the poles have a low damping. This slows down the dynamic response, as shown in Fig. 11c, which is not acceptable for the operation of the offshore converter.

When the system is unstable the resonant frequency is located in the negative-resistance region of Z_c^h, as shown in Fig. 12a. Following the Nyquist criterion, the Nyquist curve encircles $(-1, 0)$ in clockwise direction and the open loop system does not have unstable poles. Therefore, the system is unstable because the total number of zeros with positive real part is 1. In Fig. 12c, the voltage at POC shows oscillations at 309 Hz due to the resonance instability identified in Fig. 12a.

B. Connection of Wind Turbines

When the WTs are connected to the offshore ac grid, the WT converters modify the low frequency resonance location and the total damping. The stability conditions are discussed,

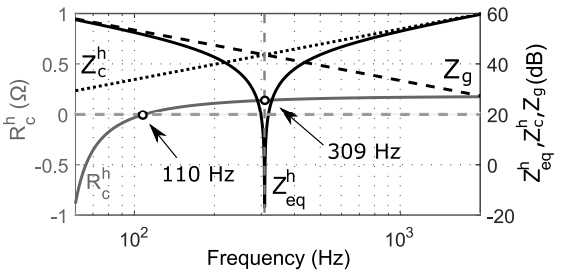

(a) Frequency response: R_c^h, Z_{eq}^h, Z_c^h, Z_g.

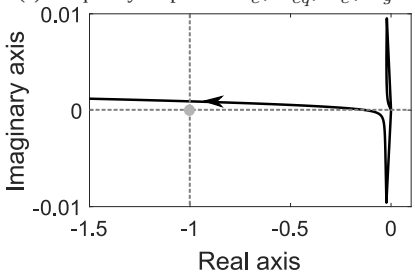

(b) Nyquist curve of Z_c^h/Z_g (positive freq.).

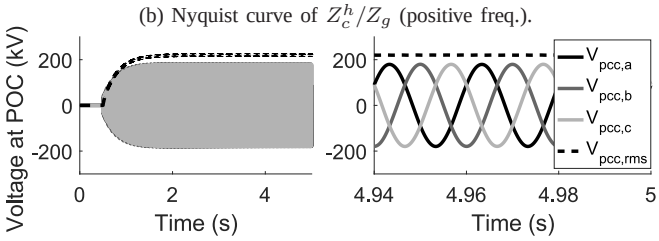

(c) Instantaneous and RMS voltages at POC. Step change is applied at 1 s

Fig. 11. Stable example in no-load operation with $k_{p,v} = 0.1$, $k_{i,v} = 3$ and $l_{cb} = 10$ km.

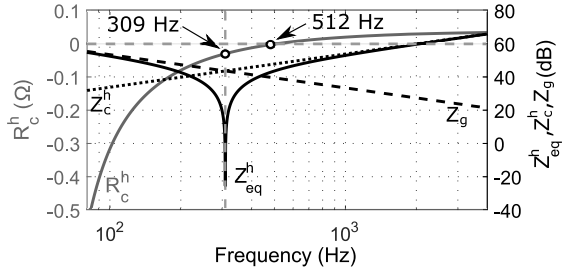

(a) Frequency response: R_c^h, Z_{eq}^h, Z_c^h, Z_g.

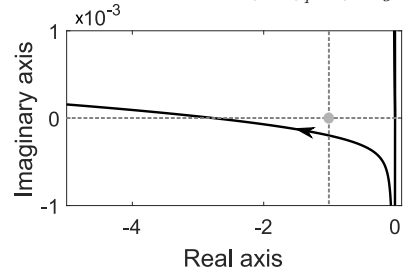

(b) Nyquist plot of Z_c^h/Z_g (pos freq.).

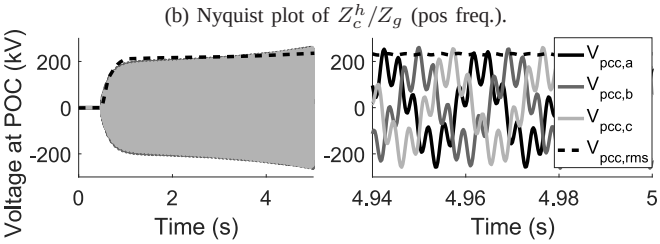

(c) Instantaneous and RMS voltages at POC. Step change is applied at 1 s

Fig. 12. Unstable example in no-load operation with $k_{p,v} = 0.1$, $k_{i,v} = 5$ and $l_{cb} = 10$ km.

This article has been accepted for publication in a future issue of this journal, but has not been fully edited. Content may change prior to final publication. Citation information: DOI 10.1109/TPWRS.2017.2663111, IEEE Transactions on Power Systems

but the expressions for the zero-crossing frequencies of R_T are not obtained analytically due to the complexity of the system.

Fig. 13 shows the stable area defined by $R_T(\omega_{res}) > 0$. There is a significant increase of the stable region when the WTs are connected. Therefore, the ac control parameters can be modified for a larger range of values to improve the dynamic response without compromising stability.

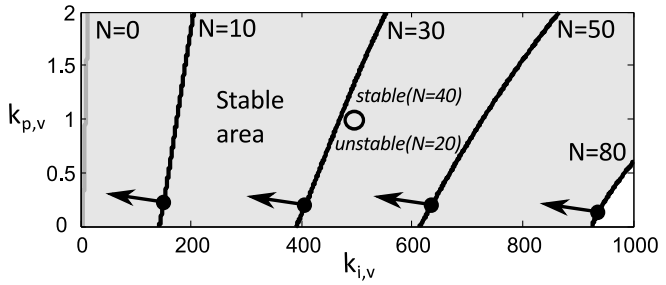

Fig. 13. Stable area of offshore HVDC converter as a function of $k_{p,v}$ and $k_{i,v}$ and the number of connected WTs (the stable and unstable examples of Fig. 15 and 16 are marked with a circle).

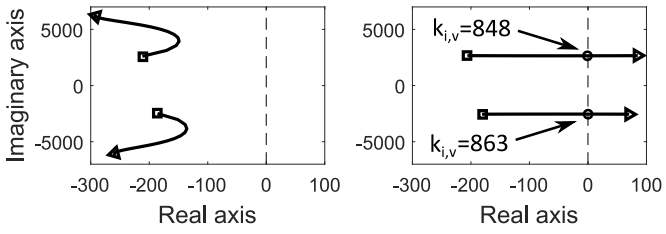

(a) Variation of $k_{p,v}$ from 0 to 80 ($k_{i,v} = 3$, $N = 80$)

(b) Variation of $k_{i,v}$ from 1 to 1200 ($k_{p,v} = 0.1$, $N = 80$)

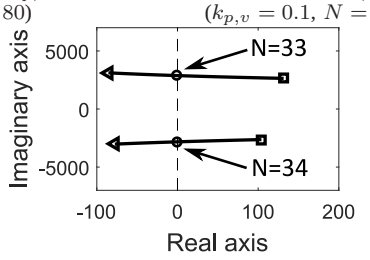

(c) Variation of WTs from 1 to 80 ($k_{p,v} = 1$, $k_{i,v} = 500$)

Fig. 14. Root locus of OWPP for variations of ac voltage control parameters and number of WTs ($N = 80$).

Fig. 14 shows the root locus of the low frequency resonant poles for different ac voltage control parameters and number of WTs. The connection of WTs improves the resonance stability because the associated poles move to the left hand side of the real axis and increase the damping of those low frequency modes. This damping contribution of the WTs is also mentioned in [2]. The stability conditions of the resonant poles agree with the stable area shown in Fig. 13. Also, the resonance moves to higher frequencies when $k_{p,v}$ and the number of WTs increases, as shown in Fig. 14.

Figs. 15-17 describe two situations where the ac voltage control is designed to have a fast dynamic response (*e.g.* $k_{p,v} = 1$ and $k_{i,v} = 500$) and the number of WTs decreases from 40 to 20. When all the WTs are connected, the offshore converter is stable because the resonance is located in a positive-resistance region, as shown in Fig. 15a. The converter introduces a negative resistance at the resonant frequency, but

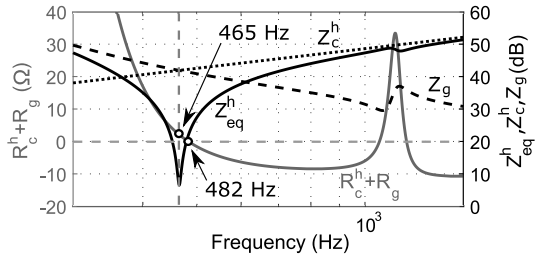

(a) Frequency response of $R_c^h + R_g$, Z_{eq}^h, Z_c^h and Z_g

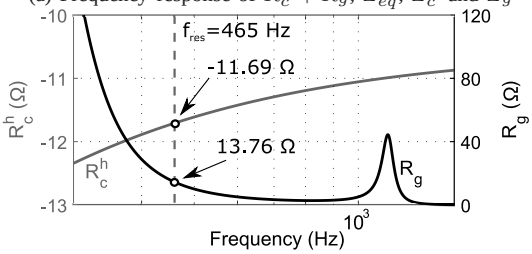

(b) Frequency response of R_c^h and R_g

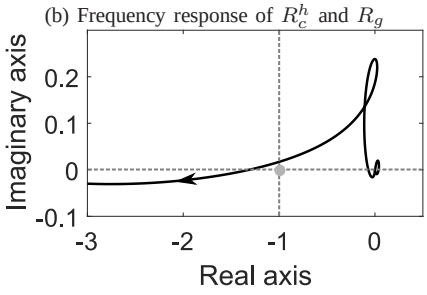

(c) Nyquist plot of Z_c^h/Z_g (positive freq.)

Fig. 15. Stable example when 40 WTs are connected, $k_{p,v} = 1$ and $k_{i,v} = 500$.

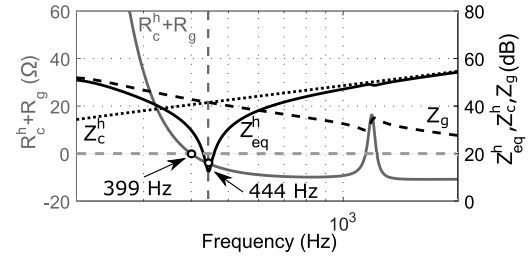

(a) Frequency response of $R_c^h + R_g$, Z_{eq}^h, Z_c^h and Z_g.

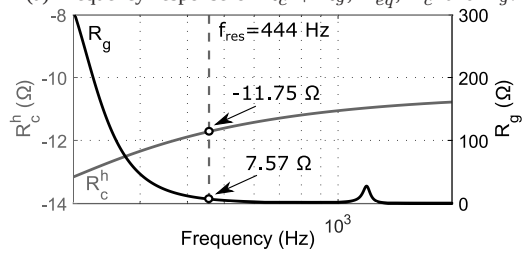

(b) Frequency response of R_c^h and R_g

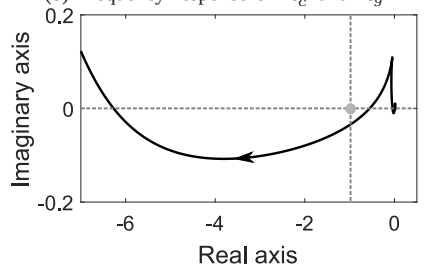

(c) Nyquist plot of Z_c^h/Z_g (positive freq.)

Fig. 16. Unstable example when 20 WTs are connected, $k_{p,v} = 1$ and $k_{i,v} = 500$.

the total damping is compensated by R_g, as shown in Fig. 15b. When the number of WTs reduces to 20 the offshore converter becomes unstable since the resonance lies in the negative-resistance region, as shown in Fig. 16a. In this case, R_g cannot compensate R_c^h, as shown in Fig. 16b. Also, the Nyquist curve agrees with the positive-net-damping criterion in both situations (Figs. 15c and 16c). In Fig. 17, the instantaneous voltages at POC show oscillations at 444 Hz when the number of WTs is reduced at 1 s; this is due to the resonance instability identified in Fig. 16a.

The variation of connected WTs can be caused by switching configurations during commissioning phases or during outages due to maintenance or contingencies [3]. As shown by the previous examples, a sudden reduction in the number of WTs should be carried out with care as this can lead to instability. Active damping can be implemented as a virtual resistor in the offshore HVDC converter to compensate the negative resistance introduced by the ac voltage control for all operational states. This will allow a design of the ac voltage control to have a fast dynamic response without compromising the stability.

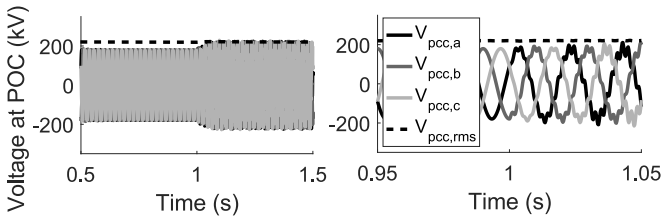

Fig. 17. Instantaneous and RMS voltages at POC when the number of WTs is reduced from 40 to 20 at 1 s. The ac voltage control parameters are $k_{p,v} = 1$ and $k_{i,v} = 500$

VII. Conclusion

Instabilities in BorWin1 have increased interest in electrical resonance interactions in HVDC-connected OWPPs. The CIGRE Working Groups suggest that series resonances can be found in the range of a few hundred Hz. These resonances can interact with the offshore HVDC converter control leading to system instability.

This paper has reformulated the positive-net-damping criterion to define the conditions of stability of an HVDC-connected OWPP as a function of the ac voltage control parameters of the HVDC converter and the configuration of the OWPP. The modified criterion is evaluated for electrical series resonances based on the phase margin condition. This reduces the complexity of the stability analysis. In addition, expressions for the low frequency resonance are obtained from simplified VSC and cable models.

Risk of detrimental resonance interaction increases in no-load operation and when a limited number of WTs are connected. This is due to the poor damping exhibited by the series resonance of the offshore grid and the resonance location at the lowest frequencies. The HVDC converter reduces the total damping at the resonant frequency if the control is designed to have a fast dynamic response. Resistive elements or active damping are necessary to compensate the negative resistance of the converter control for all possible operational states and to allow a fast dynamic response.

Appendix A

If $R_c^h(\omega) \ll X_c^h(\omega)$ and $R_g(\omega) \ll X_g(\omega)$, the loop transfer function is approximated as $L(j\omega) \approx X_c^h(\omega)/X_g(\omega)$ and its derivative as a function of ω is:

$$\frac{d|L(j\omega)|}{d\omega} \approx \frac{1}{|X_g(\omega)|^3}\frac{d|X_c^h(\omega)|}{d\omega} - \frac{|X_c^h(\omega)|}{|X_g(\omega)|^2}\frac{d|X_g(\omega)|}{d\omega} \quad (34)$$

Specific conditions for $\frac{d|L(j\omega)|}{d\omega}$ can be defined depending on the offshore grid and HVDC converter impedances:

- If the offshore grid impedance is inductive, $X_g > 0$, and the HVDC converter impedance is capacitive, $X_c^h < 0$:

$$\frac{d|X_g(\omega)|}{d\omega} > 0 \;\&\; \frac{d|X_c^h(\omega)|}{d\omega} < 0 \Rightarrow \frac{d|L(j\omega)|}{d\omega} < 0 \quad (35)$$

- If the offshore grid impedance is capacitive, $X_g < 0$, and the HVDC converter impedance is inductive, $X_c^h > 0$:

$$\frac{d|X_g(\omega)|}{d\omega} < 0 \;\&\; \frac{d|X_c^h(\omega)|}{d\omega} > 0 \Rightarrow \frac{d|L(j\omega)|}{d\omega} > 0 \quad (36)$$

Appendix B
OWPP description

A 480 MW OWPP is considered in this study. A total number of 80 WTs is distributed in 16 strings of 5 units.

Offshore HVDC VSC: MMC-VSC; rated power, 560 MVA; rated voltage, 320 kV; arm inductance, $L_{arm} = 183.7$ mH.

Offshore HVDC transformer: 2 units in parallel; rated power, 280 MVA; rated voltages, 350 kV/220 kV; equivalent inductance and resistance at 220 kV, $L_{tr}^h = 99.03$ mH, $R_{tr}^h = 0.86\ \Omega$.

Export cables: 2 cables in parallel; length, $l_{ec} = 10$ km; equivalent lumped parameters per cable, $L_{ec} = 4$ mH, $R_{ec} = 0.32\ \Omega$, $C_{ec} = 1.7\ \mu$F.

Collector transformers: 4 units in parallel; rated power of each unit, 140 MVA; rated voltages, 220 kV/33 kV; equivalent inductance and resistance of the transformers at 220 kV, $L_{tr}^{cs} = 20.63$ mH, $R_{tr}^{cs} = 0.22\ \Omega$.

WT transformers: rated power, 6.5 MVA; rated voltages, 33 kV/0.9 kV; equivalent inductance and resistance at 33 kV, $L_{tr}^{w} = 31$ mH, $R_{tr}^{w} = 1.46\ \Omega$.

WT grid side VSC: 2-level VSC; rated power, 6.5 MVA; rated voltage, 0.9 kV; coupling inductance, $L_f^w = 50\ \mu$H; coupling resistance, $R_f^w = 0.02$ mΩ; equivalent capacitance of high frequency filter, $C_f^w = 1$ mF; low pass filter bandwidth, $\alpha_f = 50$; current control bandwidth, $\alpha_c = 1000$.

References

[1] T. Thomas, "Troubleshooting continues," 2014. [Online]. Available: http://www.offshorewindindustry.com/news/troubleshooting-continues

[2] C. Buchhagen, C. Rauscher, A. Menze, and J. Jung, "BorWin1 - First Experiences with harmonic interactions in converter dominated grids," in *Int. ETG Congr. 2015; Die Energiewende - Blueprints for the new energy age*, Bonn, 2015, pp. 1–7.

[3] Working Group B3.36, "Special Considerations for AC Collector Systems and Substations Associated with HVDC - Connected Wind Power Plants," CIGRE, Tech. Rep. March, 2015.

[4] Working Group B4.55, "HVDC Connection of Offshore Wind Power Plants," CIGRE, Tech. Rep. May, 2015.

[5] A. Abdalrahman and E. Isabegovic, "DolWin1 - Challenges of connecting offshore wind farms," in *2016 IEEE International Energy Conference (ENERGYCON)*. IEEE, apr 2016, pp. 1–10.

[6] L. Harnefors, A. G. Yepes, A. Vidal, and J. Doval-Gandoy, "Passivity-Based Controller Design of Grid-Connected VSCs for Prevention of Electrical Resonance Instability," *IEEE Trans. Ind. Electron.*, vol. 62, no. 2, pp. 702–710, Feb. 2015.

[7] M. Bradt, B. Badrzadeh, E. Camm, D. Mueller, J. Schoene, T. Siebert, T. Smith, M. Starke, and R. Walling, "Harmonics and resonance issues in wind power plants," in *2011 IEEE Power and Energy Society General Meeting*. IEEE, Jul. 2011, pp. 1–8.

[8] L. Harnefors, M. Bongiorno, and S. Lundberg, "Input-Admittance Calculation and Shaping for Controlled Voltage-Source Converters," *IEEE Trans. Ind. Electron.*, vol. 54, no. 6, pp. 3323–3334, dec 2007.
[9] H. Liu and J. Sun, "Voltage Stability and Control of Offshore Wind Farms With AC Collection and HVDC Transmission," *IEEE J. Emerg. Sel. Topics Power Electron.*, vol. 2, no. 4, pp. 1181–1189, Dec. 2014.
[10] J. Sun, "Impedance-Based Stability Criterion for Grid-Connected Inverters," *IEEE Trans. Power Electron.*, vol. 26, no. 11, pp. 3075–3078, Nov. 2011.
[11] L. Harnefors, L. Zhang, and M. Bongiorno, "Frequency-domain passivity-based current controller design," *IET Power Electron.*, vol. 1, no. 4, p. 455, 2008.
[12] G. Pinares and M. Bongiorno, "Modeling and Analysis of VSC-Based HVDC Systems for DC Network Stability Studies," *IEEE Trans. Power Del.*, vol. 31, no. 2, pp. 848–856, apr 2016.
[13] L. Harnefors, "Proof and Application of the Positive-Net-Damping Stability Criterion," *IEEE Trans. Power Syst.*, vol. 26, no. 1, pp. 481–482, Feb. 2011.
[14] G. Stamatiou and M. Bongiorno, "Stability Analysis of Two-Terminal VSC-HVDC Systems using the Net-Damping Criterion," *IEEE Trans. Power Del.*, pp. 1–1, 2016.
[15] M. Cespedes and J. Sun, "Modeling and mitigation of harmonic resonance between wind turbines and the grid," in *2011 IEEE Energy Convers. Cong. and Expo.* IEEE, Sep. 2011, pp. 2109–2116.
[16] C. L. Bak, J. Hjerrild, and L. H. Kocewiak, "Wind turbine converter control interaction with complex wind farm systems," *IET Renew. Power Gen.*, vol. 7, no. 4, pp. 380–389, Jul. 2013.
[17] L. P. Kunjumuhammed, B. C. Pal, C. Oates, and K. J. Dyke, "Electrical Oscillations in Wind Farm Systems: Analysis and Insight Based on Detailed Modeling," *IEEE Trans. Sustain. Energy*, vol. PP, no. 99, pp. 1–12, 2015.
[18] J. Lyu, X. Cai, and M. Molinas, "Frequency Domain Stability Analysis of MMC-Based HVdc for Wind Farm Integration," *IEEE J. Emerg. Sel. Topics Power Electron.*, vol. 4, no. 1, pp. 141–151, mar 2016.
[19] M. Cheah-Mane, J. Liang, N. Jenkins, and L. Sainz, "Electrical Resonance Instability Study in HVDC-Connected Offshore Wind Power Plants," in *2016 IEEE Power and Energy Society General Meeting*, Boston, 2016, pp. 1–5, [Unpublished].
[20] X. Wang, F. Blaabjerg, and W. Wu, "Modeling and Analysis of Harmonic Stability in an AC Power-Electronics-Based Power System," *IEEE Trans. Power Electron.*, vol. 29, no. 12, pp. 6421–6432, dec 2014.
[21] L. Zeni, B. Hesselbaek, P. E. Sorensen, A. D. Hansen, and P. C. Kjaer, "Control of VSC-HVDC in offshore AC islands with wind power plants: Comparison of two alternatives," in *2015 IEEE Eindhoven PowerTech*. IEEE, jun 2015, pp. 1–6.
[22] L. Harnefors, X. Wang, A. G. Yepes, and F. Blaabjerg, "Passivity-Based Stability Assessment of Grid-Connected VSCsŮAn Overview," *IEEE Journal of Emerging and Selected Topics in Power Electronics*, vol. 4, no. 1, pp. 116–125, mar 2016.
[23] A. Yazdani and R. Iravani, *Voltage-Sourced Converters in Power Systems: Modeling, Control, and Applications*. Wiley, 2010.

Marc Cheah-Mane (S'14) received the degree in industrial engineering from the School of Industrial Engineering of Barcelona (ETSEIB), Technical University of Catalonia (UPC), Barcelona, Spain, in 2013. He was a researcher in Centre d'Innovacio Tecnologica en Convertidors Estatics i Accionaments (CITCEA) from 2010 to 2013. Since October of 2013, he is pursuing a Ph.D at Cardiff University, Cardiff, Wales. His research interests include renewable energies, power converters, high-voltage direct current systems, electrical machines and microgrids.

Luis Sainz was born in Barcelona, Spain, in 1965. He received his BS degree in Industrial Engineering and his PhD degree in Industrial Engineering from UPC-Barcelona, Spain, in 1990 and 1995 respectively. Since 1991, he has been a Professor at the Department of Electrical Engineering of the UPC. His research interest lies in the areas of power quality and grid-connected VSCs.

Jun Liang (M'02-SM'12) received the B.Sc. degree in Electrical Power Engineering from Huazhong University of Science and Technology, Wuhan, China, in 1992 and the M.Sc. and Ph.D. degrees from China Electric Power Research Institute, Beijing, China, in 1995 and 1998, respectively. From 1998 to 2001, he was a Senior Engineer with China Electric Power Research Institute. From 2001 to 2005, he was a Research Associate at Imperial College, London, U.K.. From 2005 to 2007, he was a Senior Lecturer at the University of Glamorgan, Wales, U.K.. Currently, he is a Reader at the School of Engineering, Cardiff University, Wales, U.K.. His research interests include FACTS devices/HVDC, power system stability and control, power electronics, and renewable power generation.

Nick Jenkins (M'81-SM'97-F'05) received the B.Sc. degree from Southampton University, Southampton, U.K., in 1974, the M.Sc. degree from Reading University, Reading, U.K., in 1975, and the Ph.D. degree from Imperial College London, London, U.K., in 1986. He is currently a Professor and Director, Institute of Energy, Cardiff University, Cardiff, U.K. Before moving to academia, his career included 14 years of industrial experience, of which five years were in developing countries. While at university, he has developed teaching and research activities in both electrical power engineering and renewable energy.

Carlos E. Ugalde-Loo (M'02) was born in Mexico City. He received the B.Sc. degree in Electronics and Communications Engineering from ITESM, MÃl'xico (2002); the M.Sc. degree in Electrical Engineering from IPN, MÃl'xico (2005); and the Ph.D. degree in Electronics and Electrical Engineering from the University of Glasgow, Scotland, U.K. (2009). In 2010 he joined the School of Engineering in Cardiff University, Wales, U.K., and is currently a Senior Lecturer in Electrical Power Systems. His academic expertise includes power system stability and control, grid integration and control of renewables, HVDC transmission, modeling of dynamic systems, and multivariable control.